Optica Applicata, Vol. XXIX, No. 4, 1999

Applications of femtosecond laser spectroscopy from clusters to clouds

LUDGER WÖSTE

Institut für Experimentalphysik, Freie Universität Berlin, Arnimallee 14, D-14195 Berlin.

Nucleation phenomena of clusters or clouds, their stability, growth, chemical activity and optical behaviour exhibit many similarities, and striking complementary aspects can be withdrawn from the investigation of both. As a result, moder experimental and computational tools, as they were developed for cluster science, amy well be beneficial for aerosol research and vice versa. Most fascinating perspectives in this regard arise from femtosecond laser spectroscopy, where experiments, which were initially motivated by understanding the dynamics of clusters, now indicate exciting atmospheric applications like remote aerosol analysis, material-free cloud injection or the laser control of loghtnings.

1. Introduction

Scientific tools are often powerful research promoters in a number of disciplines, and frequently they establish bridges between them. Atomic and molecular beam techniques provided an example, which – at first – has strongly influenced the development of atomic physics. The palette ranges from the basic Stern–Gerlach experiment to laser cooling and Bose–Einstein condensation. Further the technique has contributed substantially to nuclear research, since it provided precise data about nuclear moments, which were retrieved from hyperfine measurements in Rabi-type experiments. The techniques have also revolutionized physical chemistry, because it allowed us to observe molecular dynamics in crossed beams under single collision conditions.

Another example for the universality of a scientific tool is mass spectrometry, which – at the beginning – allowed determination of the mass of the electron at rest and relativistically. Further it enabled the separation of isotopes and the precise determination of their mass defects. It has also become a basic analytical tool in organic chemistry, where recent applications allow the mass analysis of rather complex biological samples by employing electrospray or matrix-assisted laser desorption and ionization techniques (MALDI).

The combination of molecular beam techniques and mass spectrometry has provided a decisive breakthrough in the field of cluster research. The development of the nuclear shell model [1], the verification of a non-metal-metal transition [2], the discovery of fullerenes [3], and the observation of size-selective catalytical processes [4] would not have been accomplished without supersonic beam expansion sources

combined with mass spectrometers, in which the clusters were generated and then size-specifically detected. Most of these experiments required the additional integration of a tunable radiation source, which allowed excitation and ionization of the cluster beam at well-defined energies. In this regard the development of highly performing tunable lasers provided an important tool, which enabled selective excitation of individual rotational and vibrational molecular levels into different electronic states [5]. Then the irradiated transitions were monitored by observing the resulting ionization, which either occurred directly, or via intra-molecular energy and charge transfer, which is commonly accompanied by fragmentation cascades. The time-resolved observation of these dynamical phenomena has recently gained fascinating perspectives, which may lead to the possibility of an active control of the aforementioned reaction channels [6]. These new perspectives arose from the advent of ultrafast tunable laser systems, which allow us not only to probe the intramolecular dynamics on a real-time basis, but eventually even to control it.

Laser spectroscopy has also provided an important impact to atmospheric science. The development of lidar-techniques (Ligt Detection and Ranging) is a good example. It allows, for example, the fluorescence of alkaline atoms of meteoritic origin to be detected at altitudes ranging about 90–110 km [7]. From these signals precise temperature profiles can be retrieved. At lower altitudes, where fluorescence methods fail due to the higher ambient pressure, the DIAL-method (Differential Absorption Lidar) allows us to establish at a distance of over several kilometres 3-dimensional concentration maps of atmospheric constituents such as H_2O, O_3, SO_2, NO_x, benzene, toluene, methane, *etc.* [8]. The detection limit – depending on absorption cross-section, spatial resolution and weather conditions – reaches the ppb-range (part per billion), which is an important level for tracing atmospheric pollutants. The lidar also allows us to detect aerosols, ice particles, dust and clouds [9]. Their abundance, morphology and size distribution can be determined from the lidar data at altitudes which reach even up to the stratosphere (<28 km). There the detection of stratospheric aerosols is extremely important with regard to the ozone depletion process, which mainly occurs in polar regions on the surface of the so-called PSC-particles (Polar Stratospheric Clouds) [10]. Besides, aerosols play also an important role in the chemistry of the troposphere. Examples are the creation of summer smog and the formation of acid rain. Details of these processes are not well understood. Their investigation is handicapped by the fact that the specific environment is hard to access without disturbing it. The exact characterisation of the complex heterogeneous photo-chemical reactions involved can provide the necessary input parameters, which are required for the development of precise numerical models, that will allow reliable predictions and set the basis for optimum counter-measures.

The heterogeneous photo-chemical reactions which occur on the surface of aerosols exhibit striking similarities with cluster reactions occurring on the surface of microcrystals. An example is the elementary photographic process [11]. It shows that experimental and computational concepts, as they were developed in cluster science, may very well serve for the investigation of basic heterogeneous proces-

ses in the atmosphere. In this paper, we would like to point out the analogies between both fields emphasizing that the toolbox of cluster science can be extremely useful for atmospheric research and vice versa. A most important tool in this regard is ultrafast laser spectroscopy.

2. Nucleation process

The most important process in the formation of cluster is the adiabatic beam expansion, where a gas at high stagnation pressure is expanded though a small orifice into the vacuum. As a result, a highly supersaturated system is generated in the expansion zone right behind the nozzle. In this zone multiple collisions occur among the expanded gas particles, which leads to the formation of clusters [12]. A similar phenomenon is clearly visible in the sky as condensation stripes of jet

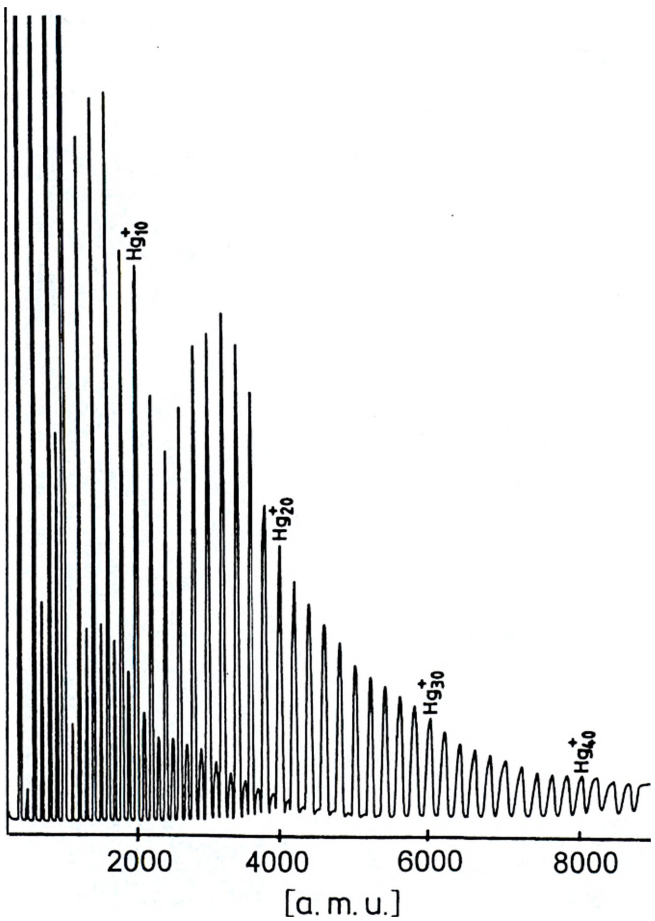

Fig. 1. Mass spectrum of mercury clusters produced in a supersonic beam expansion, ionized with VUV-synchrotron light and mass-analyzed with quadrupole mass filter. The size-distribution of simply and doubly charged particles are well recognizable [13].

aeroplanes. In the cluster experiment the use of a skimmer allows extraction of a collimated beam from the gas expansion zone. The size distribution of the particles in this beam is easily measured with a mass spectrometer. An example is given in Fig. 1, where the size distribution of a mercury cluster beam is shown. The mass spectrum was recorded with a quadrupole mass spectrometer of an extended mass range ($m/e \leqslant 10{,}000$); for this purpose the cluster beam was ionized with the tunable light of a synchrotron radiation source via inner-shell excitation followed by Auger autoionization [13]. A pronounced cluster size distribution of Hg_n clusters ($2 \leqslant n \leqslant 50$) is observable. It appears in the mass spectrum as a simply and doubly ionized distribution. By tuning the wavelength of the synchrotron light across the HOMOLUMO gap of the clusters at sizes Hg_n ($n \leqslant 13$) the onset of a Fermi-edge appears in the experiment, which is a clear indication that a transition from the original van der Waals character of the observed mercury clusters to a covalent and – at still larger sizes – metallic behaviour occurs [2].

Spectroscopic temperature measurements of supersonic beam expansions show that the resulting cluster beam is not in thermodynamical equilibrium, because the temperature, which is associated with the kinetic energy distribution of the beam,

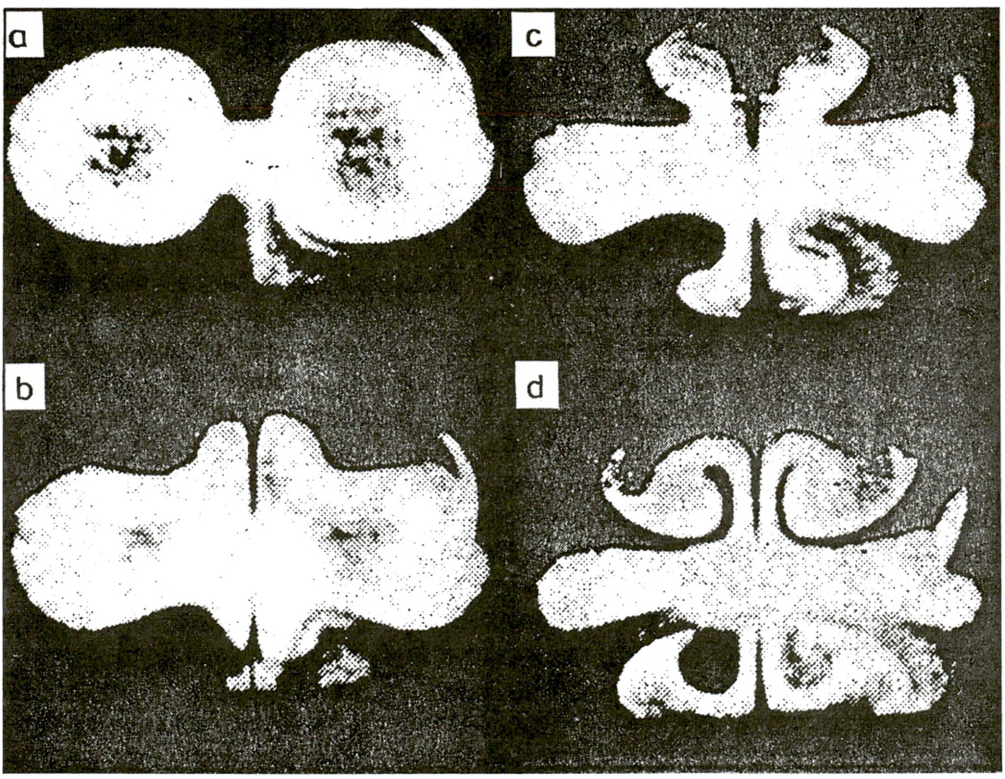

Fig. 2. Photographs of the temporal evolution (**a** – **d**) of connective patterns of "laser snow" after turning on an electric field. The aggregation was achieved by irradiating CS_2-vapour with an argon ion laser [16].

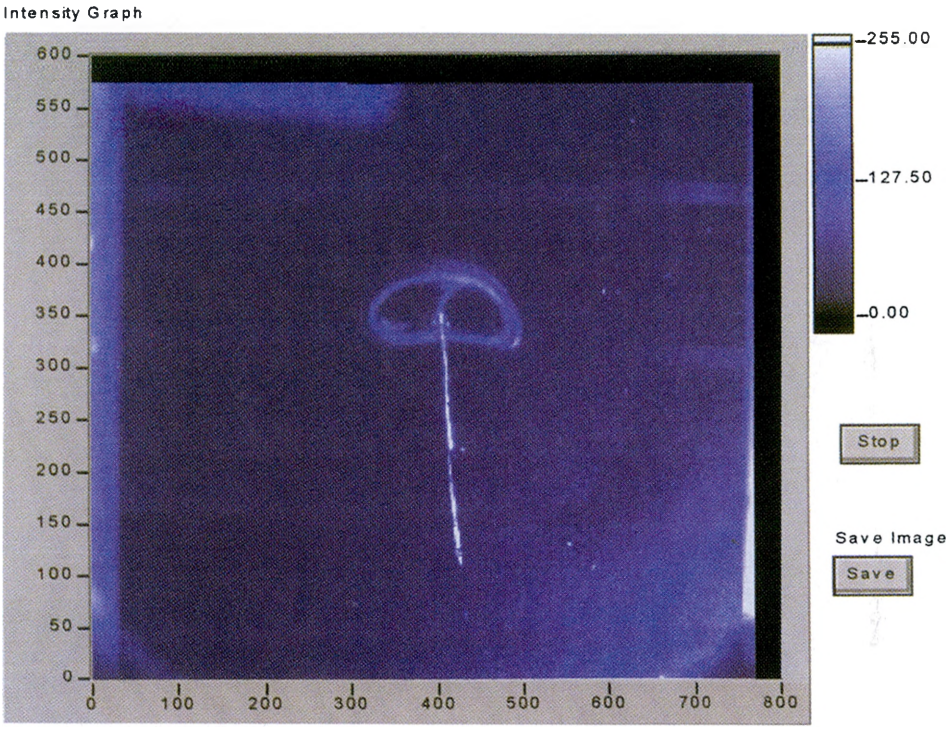

Fig. 3. Water aggregation inside a fog chamber after irradiating it with a high-intensity beam of a femtosecond laser, so multi-photon ionization occurred along the laser path [14].

differs significantly from its vibrational and rotational temperatures [14]. They strongly depend on the stagnation conditions of the beam expansion. The addition of an inert seed gas, which carries away the latent heat of cluster formation, increases the nucleation rate and stabilizes the clusters. The irradiation of the expansion zone with a resonant laser, on the other hand, can inhibit the nucleation by heating the system above its dissociative limit [15]. Under well chosen conditios, however, laser radiation may also lead to nucleation. A beautiful example – in this regard – is presented in Fig. 2. The result, obtained by ERNST and HOFFMANN [16], shows traces of the so-called "laser snow", which was generated by means of laser-induced formation of aerosols in CS_2 vapour. For the observed process the authors propose the following mechanism:

$$CS_2 + h\nu(337\ \text{nm}) \rightarrow CS_2^*,$$
$$CS_2 + CS_2^* \rightarrow 2CS + S_2,$$
$$n(CS) \rightarrow (CS)_n.$$

As a laser light source an argon ion laser was used, which resonantly excited the CS_2 vapour. A similar observation of laser-induced cluster formation was also reported by KOLWAS *et al.* [17], who found an increased aggregation of sodium clusters inside a He/Na vapour-filled heat pipe, when the system was irradiated with resonant light from an argon ion laser.

A meteorologically very important process is the nucleation of water in the atmosphere. Despite the fact that aeroplane-induced condensation stripes are the most common phenomenon, numerous unsuccessful attempts of cloud injections have been taken in the past. During these experiments silveriodide was fired with rockets into the atmosphere in order to stimulate condensation and rainfall. Evidently, however, the knowledge about suitably critical meteorological situations was still insufficient for achieving a positive result. Lidar-monitoring of the atmospheric parameters could become a helpful tool in this regard. In addition laser-induced aerosol formation – similar to the above-mentioned examples – could provide an interesting and more economic alternative to material-based cloud injections. This, however, requires excitation of adequate reactive states in air, in order to create a mechanism, which is similar to the already mentioned $(CS)_n$ or Na_n aggregation. A fascinating perspective which does allow the "transparent" atmosphere to be excited electronically is offered by novel femtosecond laser sources. Their peak intensity is sufficiently high to create a plasma by means of multiphoton ionization along the path of the laser beam [18]. These charges may then serve as nucleation germs. A photograph of aggregated water inside a fog chamber is shown in Fig. 3. The appearing fog trace was not created by the trajectory of a radioactive sample, but it was accomplished with a femtosecond laser pulse, which caused multiphoton ionization along its path [19]. Possible atmospheric applications of the observed phenomenon will be discussed in the following chapters.

3. Spectroscopic approaches

3.1. Cluster spectroscopy

Since clusters are generally produced in size distribution (see Fig. 1), mass selective observation schemes are required for withdrawing size-specific information. In this regard resonant multi-photon ionization (REMPI) has become an important tool [20]. Its simplest, two-photonic principle operates as follows. One tunable laser ($h\nu_1$) electronically excites the clusters in the beam. A second laser ($h\nu_2$), which may be the pump source for the tunable laser, is then used to ionize the excited particles, which then are recorded size-selectively with a mass spectrometer. Absorption spectra are obtained by tuning the laser $h\nu_1$ across the resonance lines of the observed particles. The size-specific observation scheme can be disturbed, however, if during the excitation or ionization step fragmentation processes occur. In this case, depletion spectroscopy, a modified version of REMPI, is employed [21]. A tunable laser $h\nu_1$ excites the particles into a dissociative state. A second laser $h\nu_2$ ionizes the resulting fragments. Simultaneously the parent ion signal is observed by probing it with a UV-laser pulse $h\nu_3$, which directly photoionizes the neutral particle beam. The signal of $h\nu_3$ provides, therefore, a monitor for the individual cluster intensities. If, however, a bound-free transition is simultaneously irradiated, a depletion of the relating parent ion signal occurs, which can then be attributed to the appearing fragment channel.

An example of electronic absorption spectra of lithium clusters Li_n ($n \leqslant 8$) is presented in Fig. 4 [22]. For the monomer it shows – as expected – the well known Li D-line. The dimer result presents the equally known vibrational progressions of the A- and B-states. The spectral sequence of the trimer exhibits pronounced pseudorotational features, as they were observed for Na_3 earlier [23]. The absorption spectrum of Li_4 still shows typical molecular features [24]. The comparison with *ab initio* calculations performed by Bonacic–Koutecky *et al.* indicates an excellent agreement between theory and experiment, from which a rhombic structure can clearly be concluded. The comparison of further calculations with the experimental results indicates that for Li_6 the first non-planar structure of a tripyramidon is adopted [25]. The spectra presented in Fig. 4 show REMPI signals for $Li-Li_3$. The spectral sequences of the larger aggregates had to be recorded by means of depletion spectroscopy. This indicates that with growing cluster size electronic bound-free transitions become dominant. However, no detailed spectral information about the excited states can be obtained from these spectra, because the excitation bands, which appear for clusters larger than Li_4, are structureless. The observed bands are, as the calculations clearly show, not yet due to the onest of plasmon resonances, although their intensity roughly scales with the number of valence electrons. The spectral locations of plasmons must appear at significantly shorter wavelengths. Such plasmon resonances were observed for larger alkali clusters by BRECHIGNAC *et al.* [26]. The situation for $Li-Li_8$, however, has still to be visualized in a molecular picture as a bunching phenomenon of a rapidly growing number of electronic states. Any spectral signature from these states is hidden by ultrafast vibronic coupling

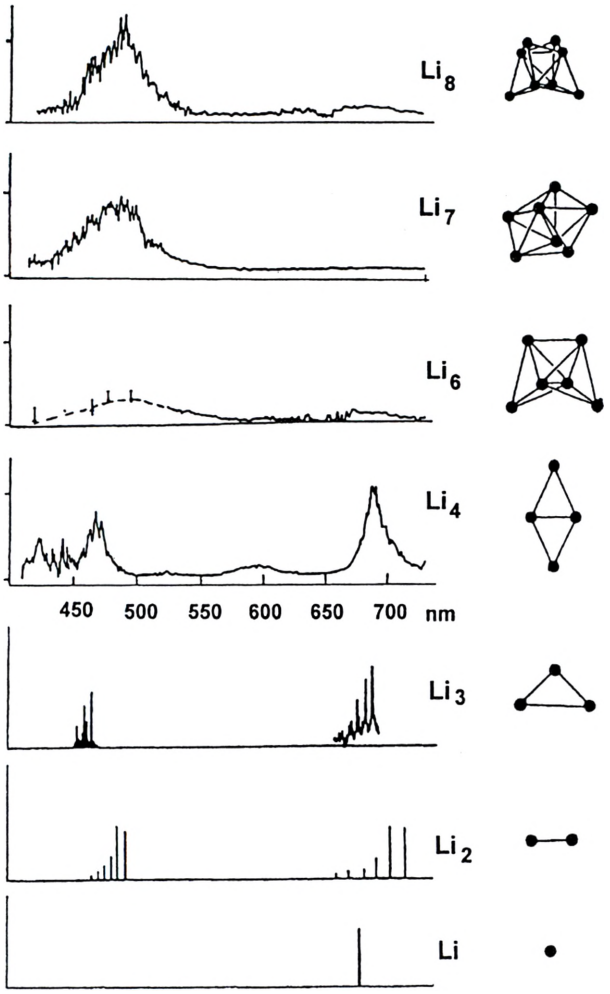

Fig. 4. Absorption spectra of Li_n clusters $1 \leqslant n \leqslant 8$. The results for $n \leqslant 3$ were recorded by means of resonant two-photon ionization, while the results for $n > 3$ were obtained by means of depletion spectroscopy. The corresponding geometries result from the comparison of the spectra with CI *ab initio* calculations [22].

phenomena and resulting fragmentation processes, which cause homogeneous line-broadening effects. In addition to that the observed bands are further broadened by isomer distributions, which may rapidly fluctuate between various configurations. Homogeneous and inhomogeneous line-broadening processes camouflage, therefore, any further analysis of the stationary spectroscopic approach. As an alternative we developed ultrafast observation schemes, which permitted us to probe the cluster dynamics in a real-time observation scheme [5].

In the time-resolved experiment an ultrafast laser pulse ($h\nu_1$ – pump) excites the particles, which then are ionized after a variable time delay with a second pulse ($h\nu_2$ – probe). The resulting ion signal is then recorded as a function of the delay

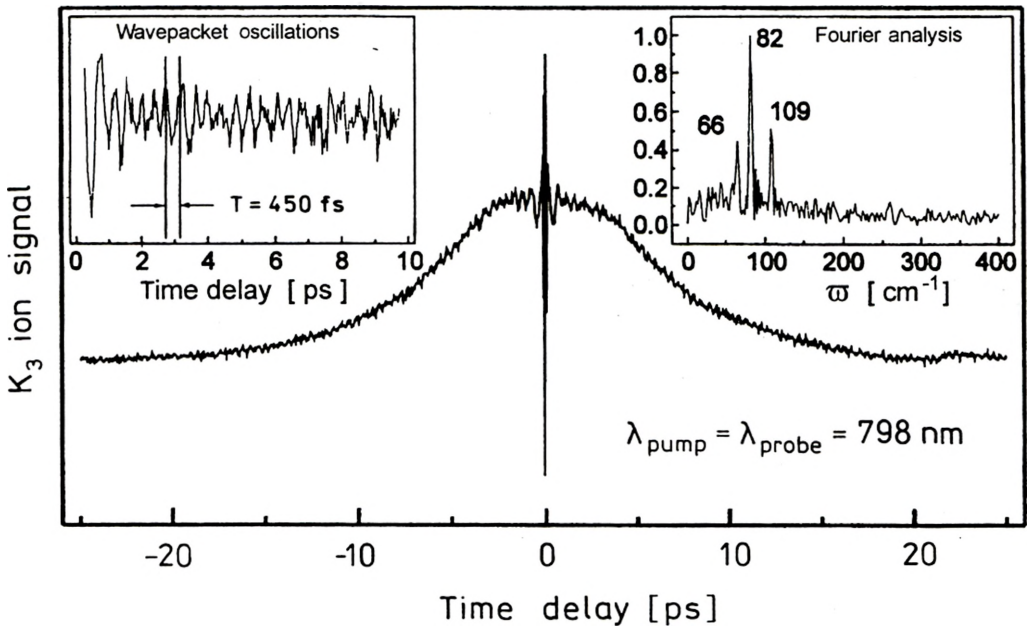

Fig. 5. Transient two-photon ionization of K_3. For $\Delta t \leqslant 10$ ps a pronounced oscillation appears, indicating the three normal vibrations (see inserts). Superposed to the vibrations a fast unimolecular decay of 450 fs decay time occurs [27].

between pump and probe. A typical result concerning the intra-molecular dynamics of photo-excited K_3 is presented in Fig. 5 [27]. The result shows a pronounced exponential decay superposed by oscillatory features. The Fourier analysis of these indicates three vibrational frequencies, which can be attributed to the symmetric stretch-, bending- and asymmetric stretch mode of the molecule. The experimental decay indicates the fragmentation of the predissociated electronic state after its excitation by the probe pulse. Meanwhile, the fragmentation patterns of various alkali clusters M_n ($n \leqslant 10$) were schematically determined [28]. An example for $Na - Na_9$ is shown in Fig. 6. The results indicate a rapidly decreasing decay time with growing cluster size, which can be attributed to the corresponding state density of the observed particle. In addition an odd-even effect is visible, which indicates a higher cluster stability for spin-paired systems.

For the ultrafast investigation of size-selected clusters in their electronic ground state the NeNePo (negative-neutral-positive) method was developed, in which negatively charged clusters were trapped in an ion trap, photo-detached into the electronic ground state of the corresponding neutral and then, after a variable delay, re-ionized to a positive ion, which then was mass-selectively detected [29]. The results trace the precise evolution of intra-molecular dynamics in photo-excited systems; they indicate the potential of ultrafast laser spectroscopy, to probe and influence bond-shaking, -breaking and -making as well as internal vibrational redistribution processes (IVR) on a real-time basis.

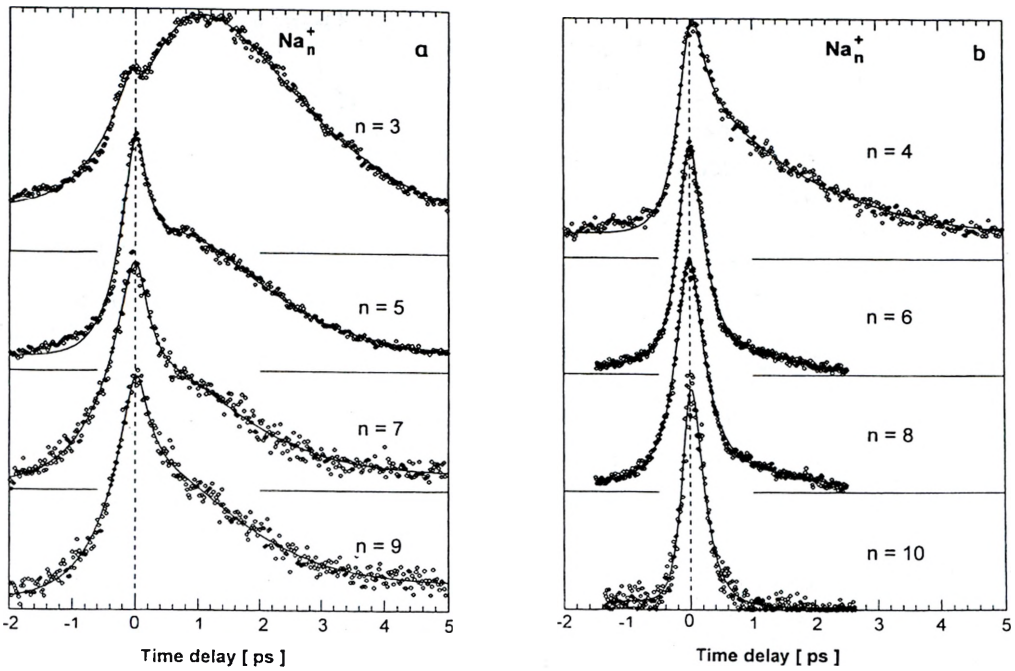

Fig. 6. Temporal evolution of the Na_n^+ signal for odd (**a**) and even (**b**) numbered clusters excited and probed with an energy $E_e = 2.94$ eV [28].

3.2. Spectroscopy on trapped aerosols

The approach of cluster spectroscopy, just to observe particles of a specific size, is still valid when particles like aerosols, which are greater than the observation wavelength, are investigated. In order to achieve this goal the use of an ion trap is again extremely helpful. For this purpose we have developed an electro-dynamical Paul trap, where the particles can be investigated individually for an unlimited amount of time [30]. As shown in Fig. 7, the quadrupole trap consists of a horizontally fixed, ring-shaped electrode and two end-cap electrodes. The ring-shaped electrode carries an AC voltage, which is adjustable from 0.5 to 6 kV at frequencies between 10 and 1000 Hz. The gravitational force of a trapped particle is compensated by a DC voltage on the end-cap electrodes. All electrodes have hyperbolically shaped surfaces. Charged microdroplets can be injected from liquids into the Paul trap by using a piezo-driven particle generator, which also ionizes the injected particles. Typically about 10^6 charges are accumulated upon each micro-droplet. The trapped particle is then illuminated with light from a linearly-polarized helium-neon laser operating at $\lambda = 632.8$ nm, which causes pronounced Mie-scatter features. The angular-resolved scatter signal is then detected with a CCD camera. It covers an angular range between 80° and 100° relative to the incident laser beam. The particle evaporates during its observation leading to a non-constant position of the droplet inside the trap. In order to compensate for this, the vertical position

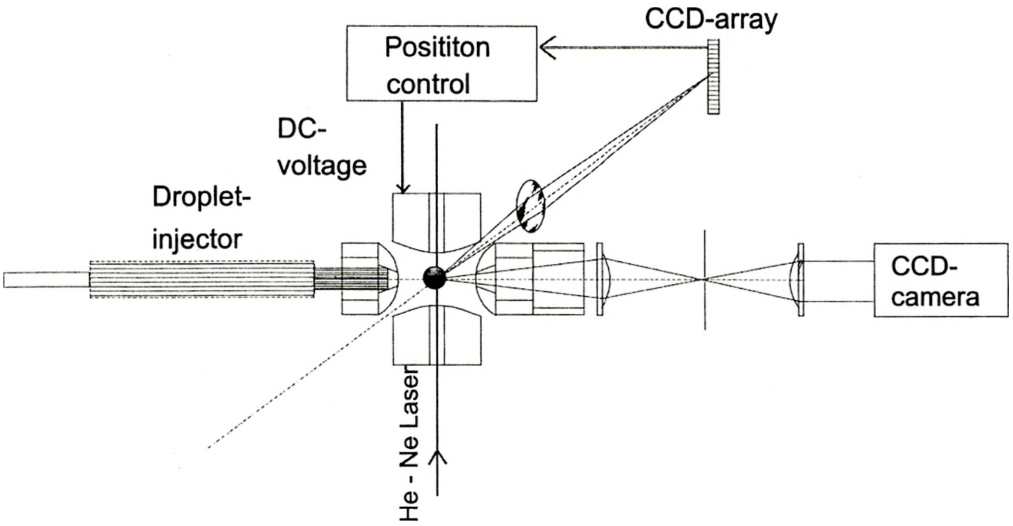

Fig. 7. Schematic diagram of the electrodynamic Paul trap for confining and investigating an injected microdroplet [30].

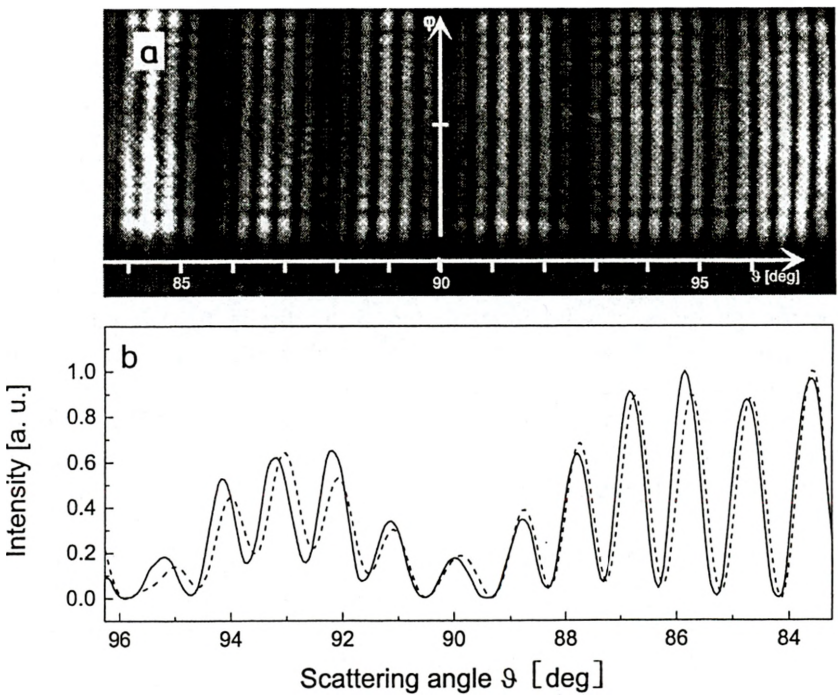

Fig. 8. Mie-pattern of a trapped microdroplet: **a** — directly measured with the CCD camera (see Fig. 7), **b** — comparison of the experimental data with Mie-theory, from which a precise determination of the particle diameter and refractive index can be given: $d = 39.81$ μm, $n = 1.4069$.

of the particle is permanently controlled by detecting the scattered light with an additional CCD line. From this position measurement a control DC voltage is applied to the end-cap electrodes to centre the particle in the trap. The voltage provides, in addition, a precise measure of the charge over mass ratio (q/m) of the trapped particle.

The ambient gas composition, pressure and temperature of the trap environment can well be controlled. This way condensation, growth, evaporation and freezing of the trapped particle can be monitored by means of an optical analysis of the scattered light. Figure 8a shows a typical scattering pattern of a liquid water droplet recorded with a CCD camera. It exhibits a sequence of bright and dark stripes, which are due to Mie scattering of spherical particles. The size of this particle is evidently greater than the wavelength of the illuminating radiation (632.8 nm). The observed stripe pattern strongly depends on the droplet size and the corresponding refractive index. The recorded patterns are (as shown in Fig. 8b) analyzed by using classical Mie theory, which provides the size and refractive index of the observed particle within an error limit of 1%.

Figure 9 shows the light of a trapped particle before and after freezing. The initially quite regular stripe pattern exhibited by the liquid droplet is now severely disturbed due to the enhanced surface roughness of the newly frozen particle. However, the stripes are still visible at the same positions as prior to freezing. This

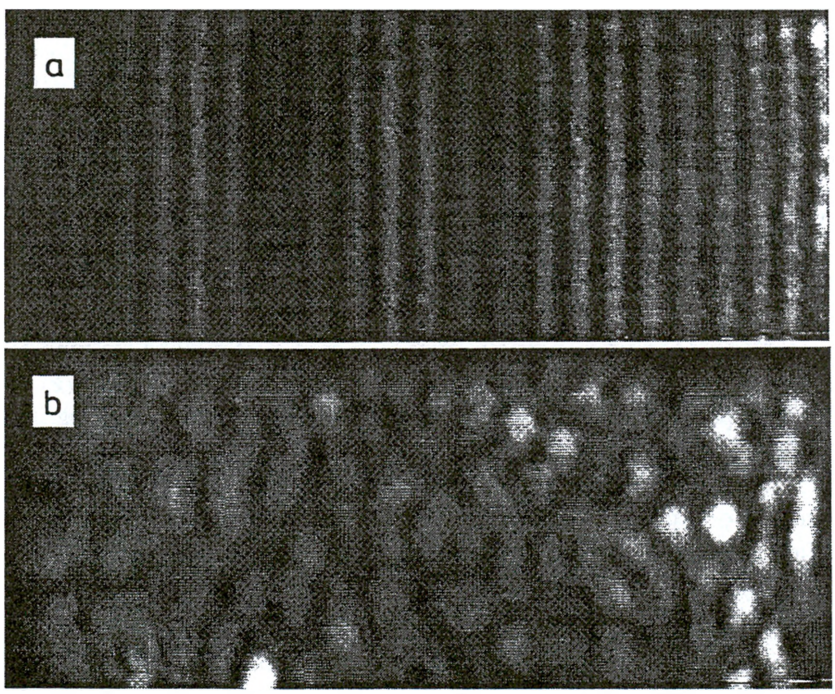

Fig. 9. Scattering pattern of a single water droplet ($T_{chamb} = -25$ °C, $p_{chamb} = 500$ mbar) liquid droplet (a), after freezing of the droplet (b). The droplet has a diameter of 50 μm [30].

indicates that the frozen particle remains close to its initially spherical shape. The observed structure is regular showing reproducible hexagonal patterns. This suggests that at least the surface of the particle contains crystalline regions.

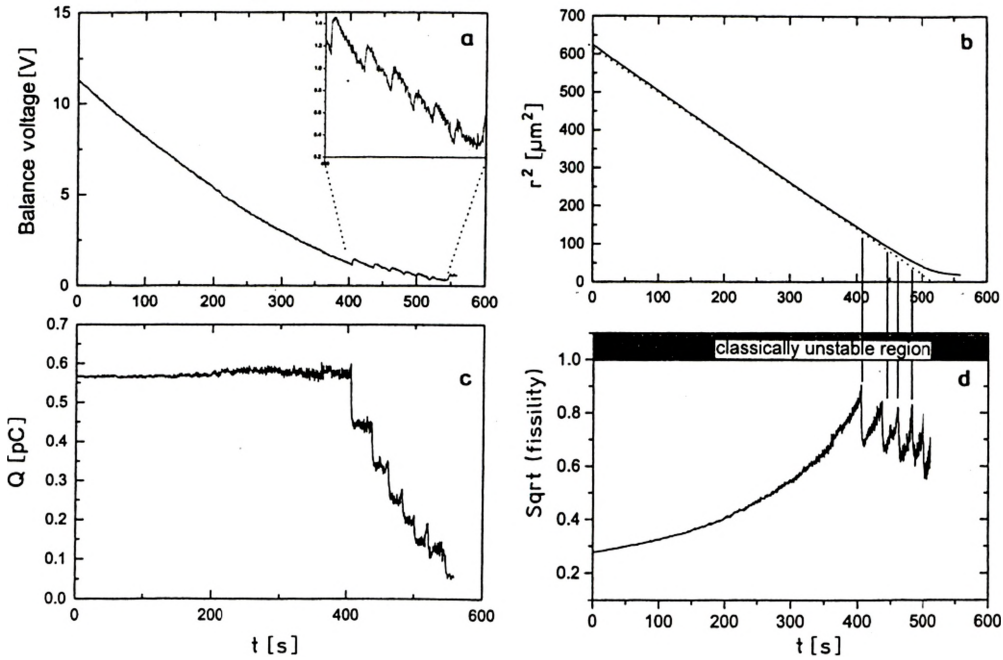

Fig. 10. Coulomb explosion of an evaporating multiply-charged microdroplet: **a** — the balance voltage indicating the q/m ratio, **b** — the (diameter)^2 retrieved from Mie scattering, **c** — the amount of total charges on the particle, **d** — the particle stability limit ($E_{coul}/2E_{surf}$), [31].

Depending on temperature and ambient gas pressure the trapped particle may grow, remain at a constant size, or evaporate, which results in corresponding changes of the Mie resonance. From these, as shown in Fig. 10**b**, precise particle diameters can be determined. The evaporation rate evidently occurs at a constant value, which is proportional to the particle surface. From the balance voltage the q/m-value of the particle is known (Fig. 10**a**). From both results (Figs. 10**a**, **b**) the total charge of the trapped particle can be retrieved. The result is plotted in Fig. 10**c**. It shows that the total charge maintains a constant value until it suddenly loses in a large step a significant part of its initial value. Later the process is repeated several times. The phenomenon can be understood as Coulomb explosion. The constantly decreasing particle diameter reaches a limit where the Coulomb energy of repulsing surface charges exceeds the surface energy [31]. As a result the particle becomes unstable and loses about 20% of its charges (see Fig. 10**c**). However, a surprising fact is that unlike the charge loss of about 20% the resulting mass loss is almost unrecognizable ($\ll 1\%$). Therefore, the process must be visualized as a sudden eruption cascade of very small charged particles from the droplet [32]. The critical limit scales with the particle diameter. The same phenomenon can also be observed

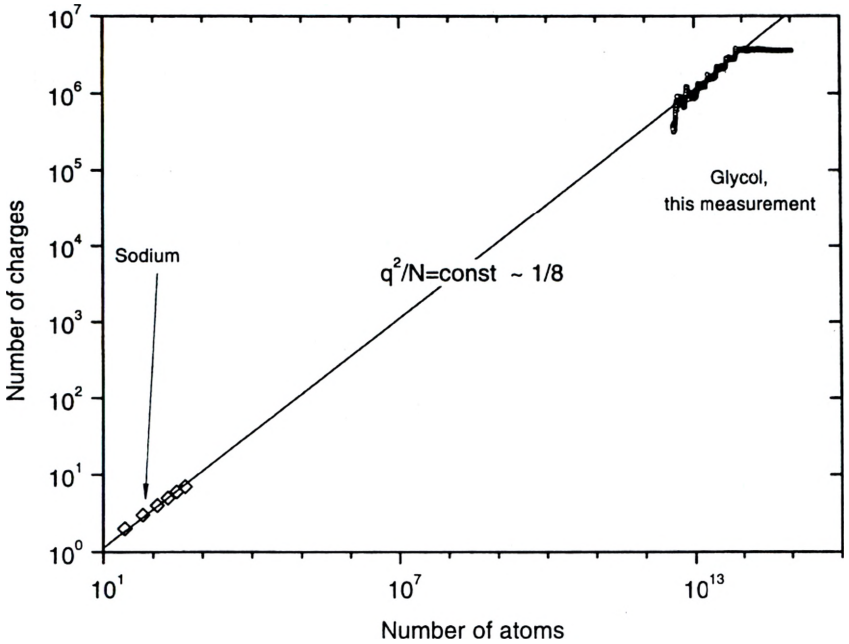

Fig. 11. Stability limits of highly charged sodium clusters and microdroplets. The linear dependence scales over 15 orders of magnitude [33].

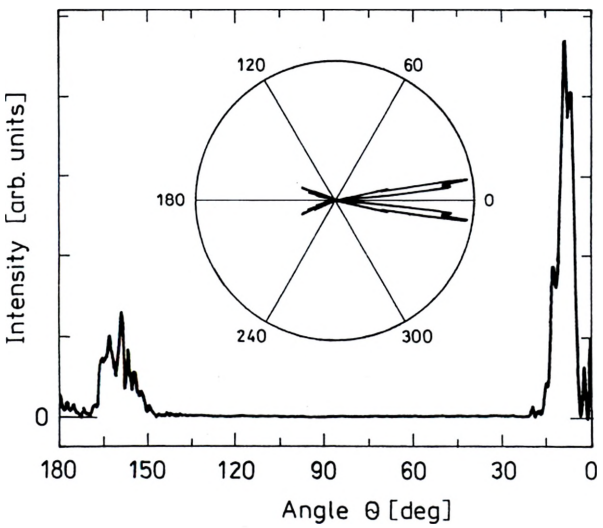

Fig. 12. Angular dependence of the third harmonic (THG) scatter intensity of microdroplet generated with femtosecond pulses. The THG scatter lobes indicate preferred forward and backward scattering [36].

with multiply charged clusters [33]. In Figure 1, for example, no doubly charged mercury clusters appear for sizes below Hg_5^{++}. Figure 11 shows that the stability limit of charged microparticles linearly scales down to the range of clusters.

The result also shows that the behaviour of microdroplets can be considered as a consequent evolution of cluster properties.

The Mie-scattered signal does contain specific spectral signatures if adequate chromophoric agents inside the trapped particle are excited. So far, Raman and fluorescence studies have successfully been carried out on single levitated microdroplets [34], [35]. The relatively weak signal, however, quickly loses intensity with the square of the observation distance, which is due to the almost isotropic scatter characteristics. For this reason, only the remote Mie-scatter analysis of aerosols (see next chapter) has been possible so far. Exciting perspectives in this regard are provided by ultrafast laser spectroscopy. Figure 12 shows an example, where a third harmonic signal (THG) in a microdroplet was generated by using a Ti:sapphire femtosecond laser. A second harmonic signal was not recorded, which is easily understood from symmetry considerations. The angular distribution of the THG-signal exhibits (as Fig. 12 shows) pronounced scatter lobes into the forward and backward direction [36]. This behaviour is completely different compared to classical Mie scattering. It can be of great importance for the lidar-analysis of aerosols.

3.3. Remote sensing of the atmosphere

The general lidar-principle is plotted in Figure 13. A laser pulse $I_0(\nu)$ is fired into the atmosphere, where it may interact by means of various processes: Rayleigh- and Raman-scattering, which mainly occur on rather abundant molecular species like N_2 and O_2, Mie scattering, which mainly occurs on aerosols, and fluorescence, which mainly occurs on meteoritic alkali dust in the mesosphere, where no more collision quenching occurs. The most important scatter process for lidar-applications is Mie scattering. It is used, for example, for the analyis of aerosols. Data obtained with a multispectral lidar system allow us to retrieve information about aerosol size distributions, their refractive index and their aggregation state [37]. An example is shown in Fig. 14, where the measurement of polar stratospheric clouds (PSC) over Sodankylä in northern Finland is shown. The PSCs are most important with respect to the stratospheric ozone depletion. On the surface of these particles reservoir species like HCl or $ClONO_2$ are deposited. In the arctic spring sunlight will dissociate these compounds and create active chloride atoms $Cl^{\bullet}$. They will react with ozone to O_2 and OCl, which then will dimerize on the PSC-surface with another OCl to $(OCl)_2$ [38]. This compound then gets photolyzed into two $Cl^{\bullet}$, while one O_2 is released. So, the catalytic O_3-destruction cycle can start again. As a result, large amounts of ozone are destroyed by just very few Cl-atoms. A full and detailed comprehension of the ozone destruction process has not yet been achieved. Laboratory experiments in a Paul trap are targeted to get a better insight. In this regard, also more information about the composition of PSC is necessary.

Information about gaseous constituents of the atmosphere can be gained if two laser wavelengths are used: one (λ_{on}) should be absorbed by the specific substance, while the other (λ_{off}) should be absorbed significantly less. A numerical analysis of the recorded backscatter signals for λ_{on} and λ_{off} then allows us to retrieve from the

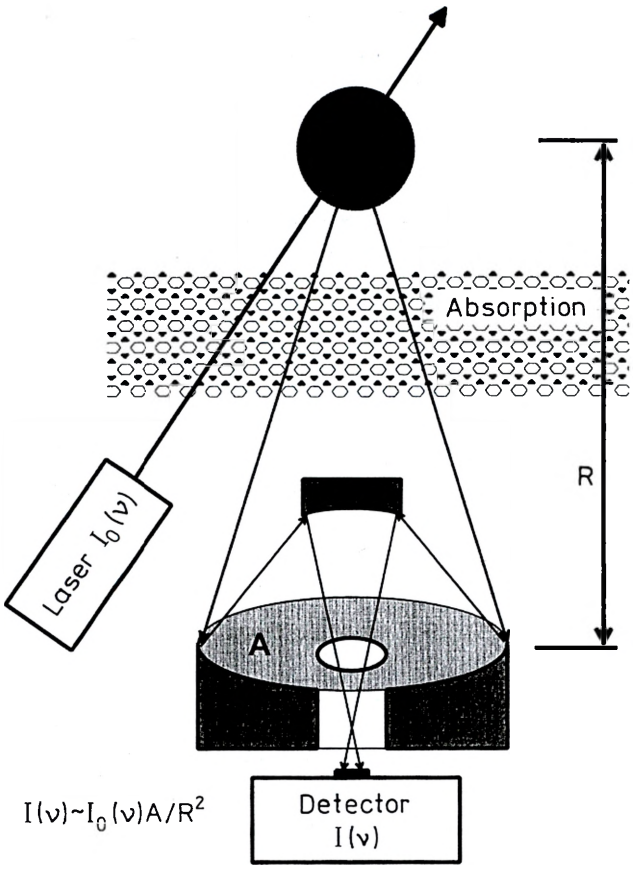

Fig. 13. Lidar principle indicating the main scatter and attenuation processes of a lidar signal. Scatter processes: Rayleigh, Mie, Raman fluorescence.

measurement the concentration of the specifically absorbed substance along the light path (Differential Absorption Lidar – DIAL). By scanning the direction of the observation 3-dimensional concentration maps of the substance in air can be gained [39]. Figure 15 shows an example of such a DIAL measurement, which was recorded on troposhperic ozone in a summer smog situation over Athens.

Although the DIAL method is a powerful tool to provide 3-dimensional information about atmospheric constituents, several aspects cannot be accomplished with the method:

- only one substance can be measured at once,
- the range is limited, due to $1/R^2$ dependence, to several kilometres,
- no information is provided about the contents of the aerosol.

These difficulties motivated us to try a lidar experiment by using a terawatt-femtosecond laser light source. Therefore, we shined the slightly focused and negatively prechirped light of a high-power fs laser (220 mJ, 100 fs) in such a manner, vertically to the sky, that the chirp and the atmospheric group velocity dispersion

just compensated each other at the location of the focus, so the shortest pulse duration was obtained there. This way a geometric and temporal focus of the beam was obtained at a distance of about 30 m from the laser. As a result atmospheric white light generation could be expected at that location. To our great surprise, however, not only a local plasma focus was generated, but an extended white light plasma channel appeared, which was clearly visible with the naked eye over an extended distance (see Fig. 16). The resulting channel light was monitored with a telescope, which was linked to an optical multichannel analyzer; it covered a wide spectral range from the UV to the IR. We detected white light signals even from altitudes of up to 12 km [40].

For the phenomenon we give the following explanation. The laser field at the location of the focus is so high that significant non.linear effects occur. First, the field-dependent non-linear refractive index creates across the Gaussian profile of the beam a Kerr lens of a focusing character. Second, the high field intensity causes multiphoton ionization. The resulting charges change the refractive index of the air across the laser beam profile in a manner of a defocusing lens. Both effects together yield to a equilibrium, which confines the initial plasma focus spatially and temporally in an extended plasma channel.

4. Outlook

The observation of an extended plasma channel created in the atmosphere by a high-power femtosecond laser gives hope for numerous fascinating applications:

– The atmospheric white light source allows us to withdraw simultaneously the spectral signatures of several atmospheric constituents in a spectral range from the UV to the IR. As a result, the range-resolved multicomponent lidar analyses can be performed. We have already demonstrated this for water absorption bands in 1000 meters altitude, from which we obtained well-resolved spectral fingerprints.

– The interaction of the high power light sources with aerosols opens up the perspective that non-linear Mie scattering will occur, causing a significantly enhanced backscatter signal to appear, which increases the range of the lidar measurements.

– The possibility of applying high light intensities to remotely located aerosols opens up further possibility that non-linear optical light emissions like stimulated Raman and plasma lines will be emitted, which should allow a multicomponent analysis of these particles.

– The high light intensity of the laser field will also enable an optical analysis of the invisible sub-micron aerosol, which is extremely important for cloud formation and the radiation balance of the earth.

– The possibility of creating charges along the laser trajectory further enables stimulation of water aggregation. This is of high importance when investigating cloud formation phenomena. Ultimately, it makes material-free cloud injections possible.

– The plasma channel is, as demonstrated, electrically conductive. This opens up the perspective to study and influence lightnings.

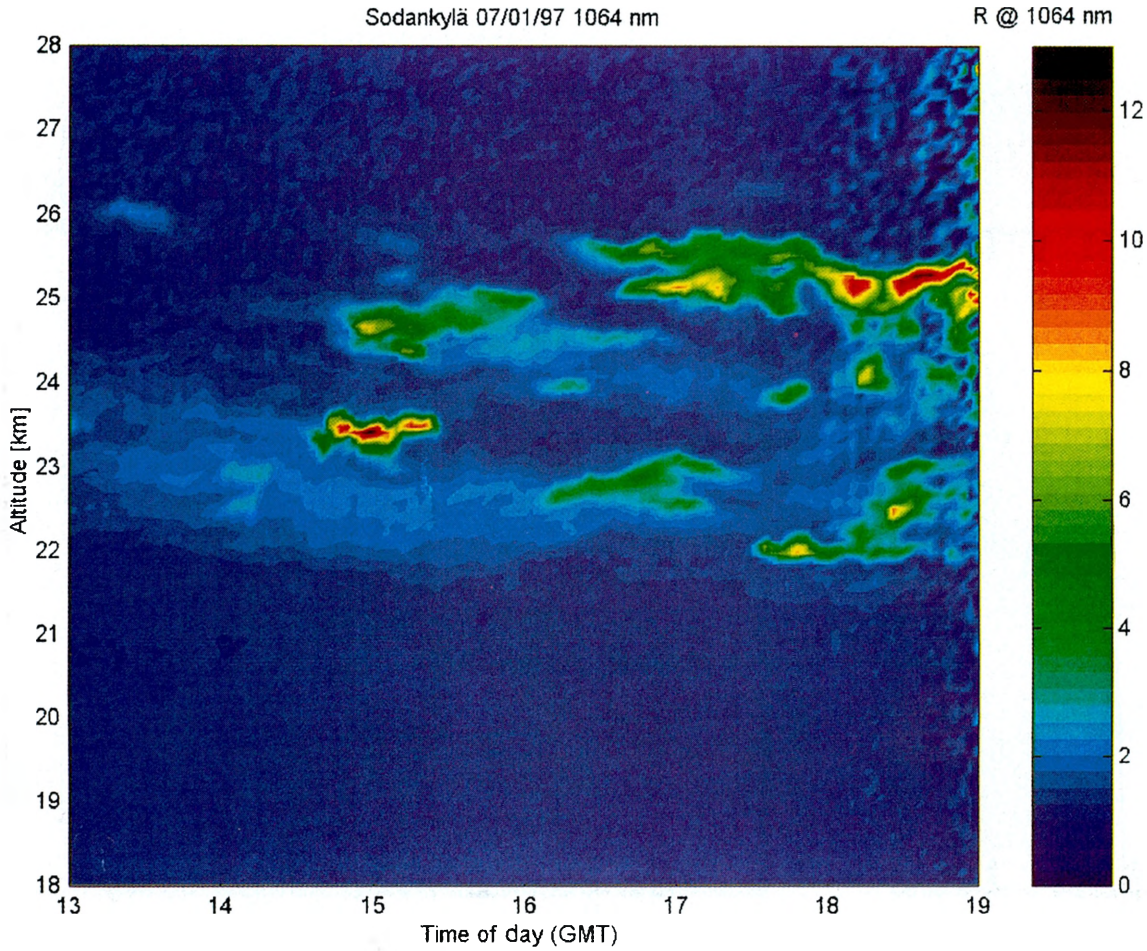

Fig. 14. PSC measured over Sodankylä (north Finland) in an altitude range 22–26 km [37].

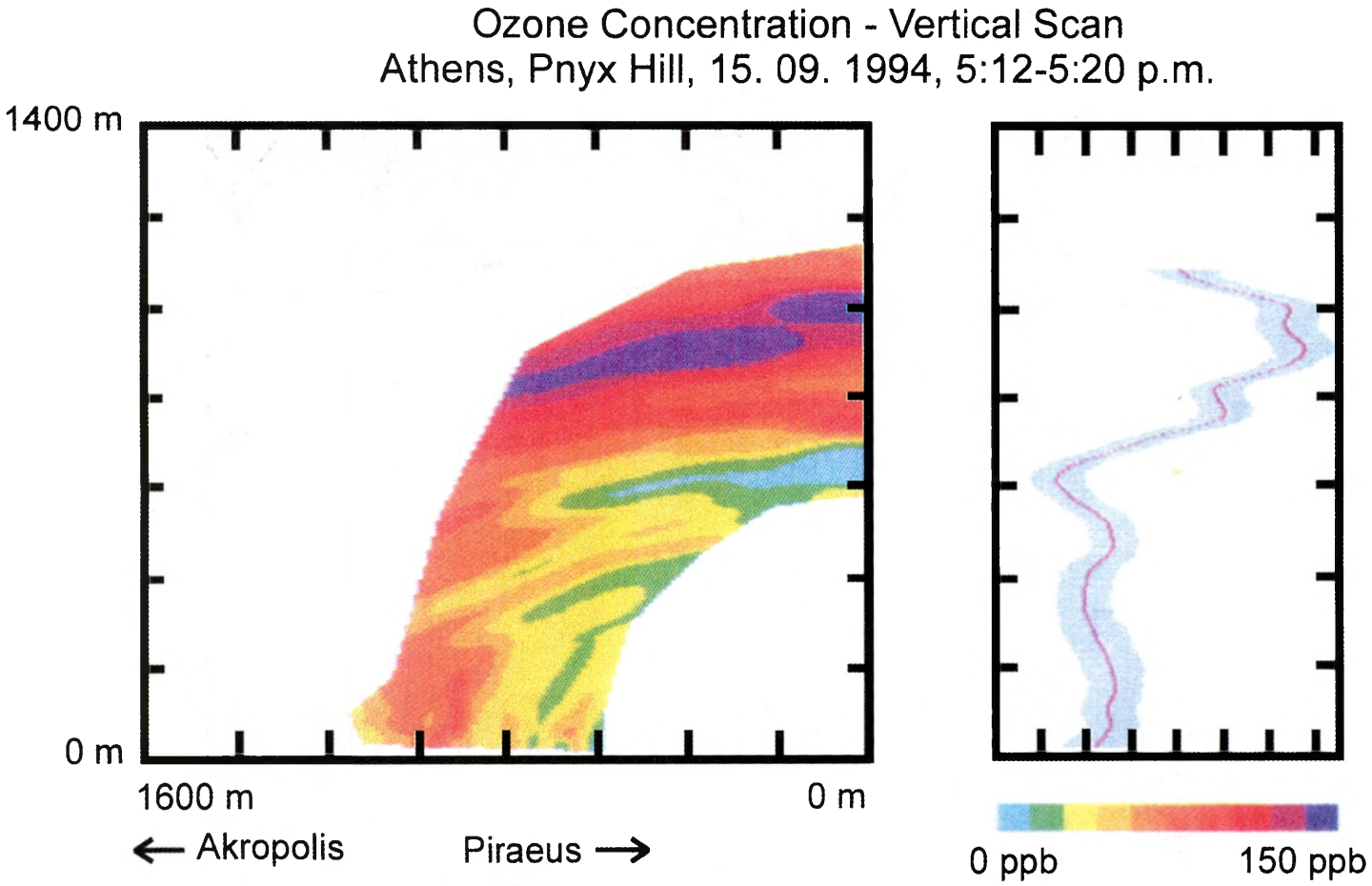

Fig. 15. Distribution of the ozone concentration over the city of Athens measured in a summer smog situation with a DIAL system [39].

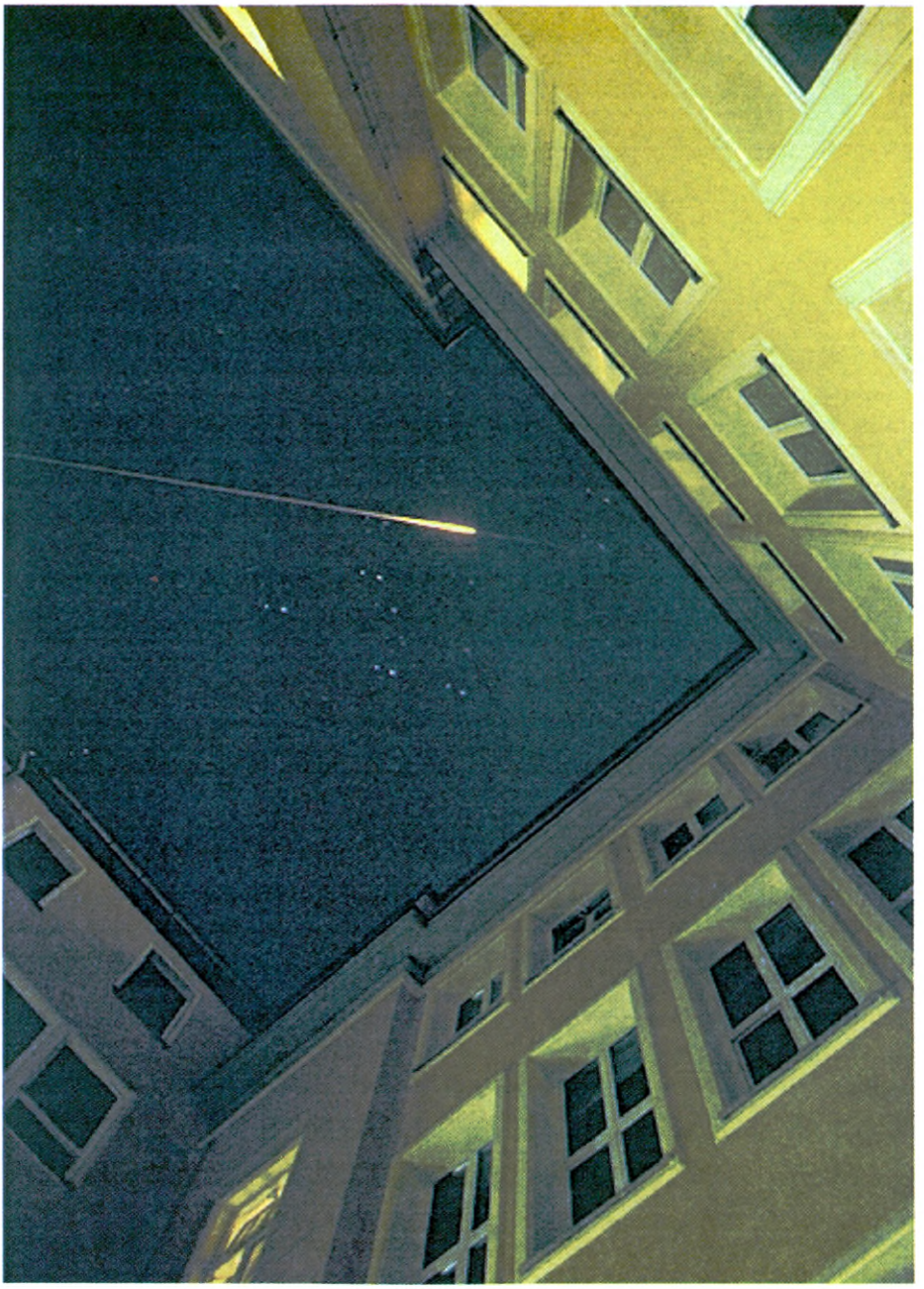

Fig. 16. Photograph of an atmospheric white light channel obtained with negatively prechirped Ti:sapphire femtosecond laser pulses (220 mJ, 100 fs). The phenomenon is clearly visible even beyond the bright planetary boundary layer. The photograph was exposed two times, as can be seen from the double appearance of the stars.

The perspectives presented originate from a basic research field, the femtosecond spectroscope of clusters. It demonstrates that the toolbox developed for this purpose can find applications in another field, the atmospheric science. As a result, there is benefit on both sides, which may even lead to a convergence, in which large water clusters will receive the same description as the sub-micron aerosol.

Acknowledgements — The work presented here was performed by my very motivated collaborators: A. Bartelt, S. Frey, F. Herb, H. Hess, O. Hübner, F. Immler, T. Leisner, J. Luderer, C. Lupulescu, M. Müller, M. Rodriguez, P. Rosendo, S. Vajda, H. Vortisch and H. Wille. Further we maintain very close scientific contacts with S. Berry, V. Bonancic-Koutecky, K. Ernst, J. Kasparian, K. Kolwas, S. Niedermayer, P. Rairoux, S. Rutz, R. Sauerbrey, H. Schillinger, E. Schreiber, M. Ulbricht, D. Weidauer and J. P. Wolf. I want to thank them for their enthusiasm, the ideas they provided and their great spirit of cooperation.

References

[1] KIGHT W., CLEMENGER K., DE HEER W., SAUNDERS W., CHOU M., COHEN M. L., Phys. Rev. Lett. **52** (1984), 2141.
[2] BRECHIGNAC C., BROYER M., CAHUZAC P., DELACRÉTAZ G., LABASTIE P., WOLF J. P., WÖSTE L., Phys. Rev. Lett. **60** (1988), 275.
[3] KROTO H. W., HEALTH J. R., O'BRIEN S. C., SMALLEX R. F., Nature **138** (1985), 165.
[4] VAJDA S., LEISNER T., WOLF S., WÖSTE L., Philos. Mag. B **79** (1999), 1353.
[5] WÖSTE L., Z. Phys. Chem. **196** (1996), 1.
[6] BERRY R. S., BONACIC-KOUTECKY V., GAUS J., LEINSER T., MANZ J., REISCH-LENZ B., RUPPE H., RUTZ S., SCHREIBER E., VAJDA S., DE VIVIE-RIEDLE R., WOLF S., WÖSTE L., Adv. Chem. Phys. **101** (1997), 101.
[7] VON ZAHN U., HÖFER J., Geophys. Res. Lett. **23** (1996), 141.
[8] WEIDAUER D., RAIROUX P., ULBRICHT M., WOLF J. P., WÖSTE L., [In] *Advances in Atmospheric Remote Sensing with Lidar*, [Eds.] A. Ansmann, R. Neuber, P. Rairoux, U. Wandinger, Springer-Verlag, 1996.
[9] KOLENDA J., MIELKE B., RAIROUX P., STEIN B., WEIDAUER D., WOLF J. P., WÖSTE L., CASTAGNOLI F., DEL GUASTA M., MORANDI M., SACCO V., STEFANUTTI L., VENTURI V., ZUCCAGNOLI L., Proc. SPIE **1714** (1992), 208.
[10] WEDEKIND C., IMMLER F., MIELKE B., RAIROUX P., STEIN B., WÖSTE L., DEL GUASTA M., MORANDI M., STEFANUTTI L., MASCI F., RIZI V., MARTHEY R., MITEV V., DOUARD M., WOLF J. P., KYRÖ E., [In] *Advances in Atmosphere Remote Sensing with Lidar*, [Eds.] R. Neuber, P. Rairoux, U. Wandinger, Springer Verlag, 1996, p. 513.
[11] LEISNER T., ROSCHE C., WOLF S., GRANZER F., WÖSTE L., Surface Rev. Lett. **3** (1996), 1105.
[12] DELACRÉTAZ G., WÖSTE L., Surface Sci. **156** (1985), 770.
[13] BLANC J., BROYER M., DUGOURD P., LABASTIE P., SENCE M., WOLF J. P., WÖSTE L., J. Chem. Phys. **102** (1995). 680.
[14] DELACRÉTAZ G., WÖSTE L., Helv. Phys. Acta **58** (1985), 883.
[15] RECHENSTEINER R., MONOT R., ZELLWEGER J. M., VAN DEN BERGH H., WÖSTE L., Helv. Phys. Acta **54** (1981), 282.
[16] ERNST J., HOFFMANN J. J., Chem. Phys. Lett. **68** (1979), 40.
[17] KOLWAS K., KOLWAS M., JAKUBCZYK D., Appl. Phys. B **60** (1995), 173.
[18] BRAUN A., KORN G., LIUS X., DU D., SQIER J., MOUROU G., Opt. Lett. **20** (1995), 73.
[19] LUDERER J. C., RODRIGUES M., WILLE H., WÖSTE L., to be published.
[20] HERRMANN A., LEUTWYLER S., SCHUMACHER E., WÖSTE L., Chem Phys. Lett. **52** (1977), 418.
[21] BROYER M., DELACRÉTAZ G., NI G.-Q., WHETTEN R. L., WOLF J. P., WÖSTE L., Phys. Rev. Lett. **62** (1989), 2100.

[22] BLANC J., BONACIC-KOUTECKY V., BROYER M., CHEVALEYRE J., DUGOURD P., SCHEUCH C., WOLF J.P., WÖSTE L., J. Chem. Phys. **96** (1992), 1793.
[23] BROYER M., CHEVALEYRE J., DUGOURD P., WOLF J.P., WÖSTE L., Chem. Phys. Lett. **225** (1994), 28.
[24] BROYER M., CHEVALEYRE J., DUGOURD P., WOLF J.P., WÖSTE L., Phys. Rev. A **42** (1990), 6954.
[25] DUGOURD P., BLANC J., BONACIC-KOUTECKY V., BROYER M., CHEVALEYRE J., KOUTECKY J., PITTNER J., WOLF J.P., WÖSTE L., Phys. Rev. Lett. **67** (1991), 2638.
[26] BRECHIGNAC C., CAHUZAC P., CARLIER F., DE FRUTOS M., LEGNIER J., Chem. Phys. Lett. **189** (1992), 28.
[27] FAYET P., WÖSTE L., Spectrosc. Int. J. **3** (1984), 91.
[28] KÜHLING H., KOBE K., RUTZ S., SCHREIBER E., WÖSTE L., J. Phys. Chem. **98** (1994), 6679.
[29] WOLF S., SOMMERER G., RUTZ S., SCHREIBER E., LEISNER T., WÖSTE L., BERRY R.S., Phys. Rev. Lett. **74** (1995), 4177.
[30] KRÄMER B., SCHWELL M., HÜBNER O., VORTISCH H., LEISNER T., RÜHL E., BAUMGÄRTEL H., WÖSTE L., Ber. Bunsenges. Phys. Chem. **100** (1996), 1911.
[31] LORD RAYLEIGH, Phil. Mag. XIV (1882), 184.
[32] KRÄMER B., Dissertation, FU-Berlin, 1997.
[33] NÄHER U., Z. Phys. D **31** (1994), 191.
[34] SCHASCHEK K., POPP J., KIEFER W., [In] Proc. XIII Intern. Conf. Raman Spectr., [Ed.] W. Kiefer, Wiley 1992.
[35] CHEUNG J.L., HARTINGS J.M., CHANG R.K., [In] *Handbook of Optical Properties*, [Ed.] R.E. HUMMEL, CRC, 1997.
[36] KASPARIAN J., KRÄMER B., DEWITZ J.P., VAJDA S., RAIROIX P., VEZIN B., BOUTOU V., LEISNER T., HÜBNER W., WOLF J.P., WÖSTE L., BENNEMANN K.H., Phys. Rev. Lett. **78** (1997), 2952.
[37] WEDEKIND C., IMMLER F., MIELKE B., RAIROUX P., STEIN B., WÖSTE L., DEL GUASTA M., MORANDI M., STEFANUTTI L., MASCI F., RIZI V., MATTHEY R., MITEV V., DOUARD M., WOLF J.P., KYRÖ E., [In] *Advances in Atmospheric Remote Sensing with Lidar*, [Ed.] A. Ansmann, R. Neuber, P. Rairoux, U. Wandinger, 513, Springer-Verlag, 1997.
[38] MOLINA L.T., MOLINA M.J., J. Phys. Chem. **91** (1987), 433.
[39] STEIN B., IMMLER F., MIELKE B., RAIROUX P., WEDEKIND C., WILLE H., WÖSTE L., [In] *Advances in Atmospheric Remote Sensing with Lidar*, [Eds.] A. Ansmann, R. Neuber, P. Rairoux, U. Wandinger, 391, Springer-Verlag, 1996.
[40] WÖSTE L., WEDEKIND C., WILLE H., RAIROUX P., STEIN B., NIKOLOV S., WERNER C., NIEDERMEIER S., RONNENBERGER F., SCHILLINGER H., SAUERBREY R., *Femtosecond Atmospheric Lamp*, AT-Fachverlag Laser und Optoelektronik, E 2688 (1977).

Received September 30, 1999